LETTER

doi:10.1038/nature14270

State preservation by repetitive error detection in a superconducting quantum circuit

J. Kelly[1]*, R. Barends[1]†*, A. G. Fowler[1,2]†*, A. Megrant[1,3], E. Jeffrey[1]†, T. C. White[1], D. Sank[1]†, J. Y. Mutus[1]†, B. Campbell[1], Yu Chen[1]†, Z. Chen[1], B. Chiaro[1], A. Dunsworth[1], I.-C. Hoi[1], C. Neill[1], P. J. J. O'Malley[1], C. Quintana[1], P. Roushan[1]†, A. Vainsencher[1], J. Wenner[1], A. N. Cleland[1] & John M. Martinis[1]†

Quantum computing becomes viable when a quantum state can be protected from environment-induced error. If quantum bits (qubits) are sufficiently reliable, errors are sparse and quantum error correction (QEC)[1–6] is capable of identifying and correcting them. Adding more qubits improves the preservation of states by guaranteeing that increasingly larger clusters of errors will not cause logical failure—a key requirement for large-scale systems. Using QEC to extend the qubit lifetime remains one of the outstanding experimental challenges in quantum computing. Here we report the protection of classical states from environmental bit-flip errors and demonstrate the suppression of these errors with increasing system size. We use a linear array of nine qubits, which is a natural step towards the two-dimensional surface code QEC scheme[7], and track errors as they occur by repeatedly performing projective quantum non-demolition parity measurements. Relative to a single physical qubit, we reduce the failure rate in retrieving an input state by a factor of 2.7 when using five of our nine qubits and by a factor of 8.5 when using all nine qubits after eight cycles. Additionally, we tomographically verify preservation of the non-classical Greenberger–Horne–Zeilinger state. The successful suppression of environment-induced errors will motivate further research into the many challenges associated with building a large-scale superconducting quantum computer.

The ability to withstand multiple errors during computation is a critical aspect of error correction. We define nth-order fault tolerance to mean that any combination of n errors is tolerable. Previous experiments based on nuclear magnetic resonance[8,9], ion traps[10] and superconducting circuits[11–13] have demonstrated multi-qubit states that are first-order tolerant to one type of error. Recently, experiments with ion traps and superconducting circuits have shown the simultaneous detection of multiple types of errors[14,15]. All of these experiments demonstrate error correction in a single round; however, quantum information must be preserved throughout computation using multiple error-correction cycles. The basics of repeating cycles have been shown in ion traps[16] and superconducting circuits[17]. Until now, it has been an open challenge to combine these elements to make the information stored in a quantum system robust against errors which intrinsically arise from the environment.

The key to detecting errors in quantum information is to perform quantum non-demolition (QND) parity measurements. In the surface code, this is done by arranging qubits in a chequerboard pattern—with data qubits corresponding to the white squares (blue in Fig. 1), and measurement qubits to the black squares (green in Fig. 1)—and using these ancilla measurement qubits to repetitively perform parity measurements to detect bit-flip ($\hat{X}$) and phase-flip ($\hat{Z}$) errors[7,18]. A square chequerboard with $(4n+1)^2$ qubits is nth-order fault tolerant, meaning that at least $n+1$ errors must occur to cause failure in preserving a state if fidelities are above a threshold. With error suppression factor $\Lambda > 1$ and more qubits, failure becomes increasingly unlikely with probability $\varepsilon \propto -1/\Lambda^{n+1}$ (assuming independent errors). The surface code is highly appealing for superconducting quantum circuits as it requires only nearest-neighbour interactions, single and two-qubit gates, and fast repetitive measurements with fidelities above a lenient threshold of approximately 99%. All of this has recently been demonstrated in separate experiments[19,20].

The simplest system demonstrating the basic elements of the surface code is a one-dimensional chain of qubits, as seen in Fig. 1a. It can run the repetition code, a primitive of the surface code, which corrects bit-flip errors on both data and measurement qubits. The device shown in Fig. 1b is a chain of nine qubits, which allows us to experimentally test both first- and second-order fault tolerance. It consists of a superconducting aluminium film on a sapphire substrate, patterned into Xmon transmon qubits[21] with individual control and readout. The qubits are the cross-shaped devices; they are capacitively coupled to their nearest neighbours, controlled with microwave drive and frequency detuning pulses, and measured with a dispersive readout scheme. The device consists of five data qubits and four measurement qubits in an alternating pattern; see Supplementary Information for details.

To detect bit-flips, we determine the parity of adjacent data qubits by measuring the operator $\hat{Z}\hat{Z}$. We do this using an ancilla measurement qubit, and performing single- and two-qubit quantum gates (Fig. 1c). The operator measurement can have two values: $+1$ for states $|00\rangle$ and $|11\rangle$, and -1 for $|01\rangle$ and $|10\rangle$. Therefore, errors can be detected as they occur by repeating this operator measurement and noting changes in the outcome. Importantly, this measurement does not destroy the quantum nature: given input $a|00\rangle + b|11\rangle$ the result will be $+1$ and the quantum state remains, with similar behaviour for other Bell-like superposition states. In the repetition code, simultaneous measurements of these operators enable multiple bit-flip errors to be detected.

We now discuss how bit-flip errors, which can occur on any qubit and at any time, are identified. The quantum circuit of the repetition code is shown in Fig. 2a, for three cycles (in time) and nine qubits. This is the natural extension of the schematic in Fig. 1c, optimized for our hardware (Supplementary Information). Figure 2a illustrates four distinct types of bit-flip errors (stars): measurement error (gold), single-cycle data error (purple), two-cycle data error (red), and a data error after the final cycle (blue). Controlled-NOT (CNOT) gates propagate bit-flip errors on the data qubit to the measurement qubit. Each of these errors is typically detected at two locations if in the interior and at one location if at the boundary; we call these 'detection events'. The error connectivity graph[22] is shown in Fig. 2b, where the grey lines indicate every possible pattern of detection events that can arise from a single error. The last column of values for the $\hat{Z}\hat{Z}$ operators in Fig. 2b are constructed from the data qubit measurements, so that errors between the last cycle and data qubit measurement can be detected (Supplementary Information).

In the absence of errors, there are two possible patterns of sequential measurement results. If a measurement qubit's neighbouring data

[1]Department of Physics, University of California, Santa Barbara, California 93106, USA. [2]Centre for Quantum Computation and Communication Technology, School of Physics, The University of Melbourne, Victoria 3010, Australia. [3]Department of Materials, University of California, Santa Barbara, California 93106, USA. †Present address: Google Inc., Santa Barbara, California 93117, USA.
*These authors contributed equally to this work.

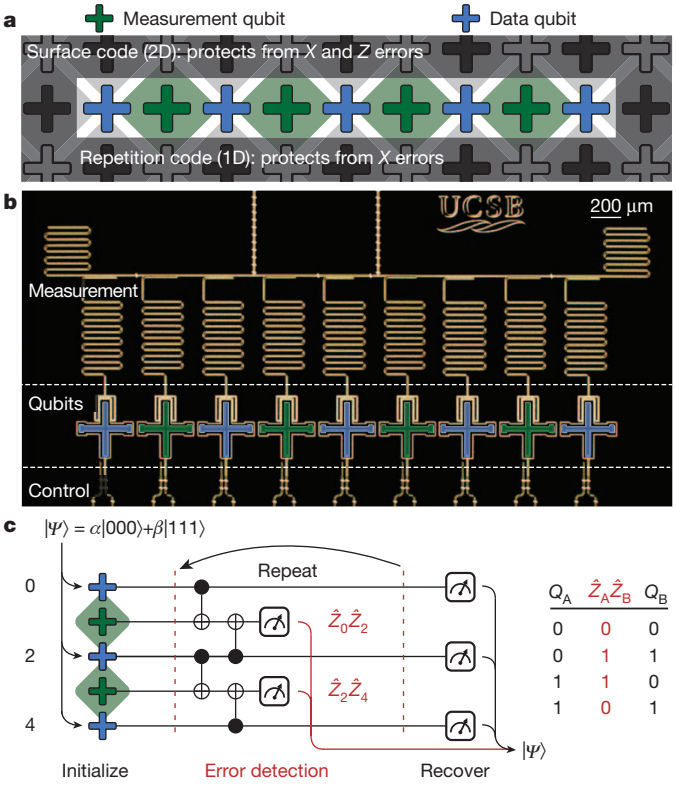

Figure 1 | Repetition code: device and algorithm. **a**, The repetition code is a one-dimensional (1D) variant of the surface code, and is able to protect against $\hat{X}$ (bit-flip) errors. The code is implemented using an alternating pattern of data and measurement qubits. **b**, Optical micrograph of the superconducting quantum device, consisting of nine Xmon[21] transmon qubits with individual control and measurement, with a nearest-neighbour coupling scheme. **c**, The repetition code algorithm uses repeated entangling and measurement operations which detect bit-flips, using the parity scheme on the right. Using the output from the measurement qubits during the repetition code for error detection, the initial state can be recovered by removing physical errors in software. Measurement qubits are initialized into the $|0\rangle$ state and need no reinitialization as measurement is QND.

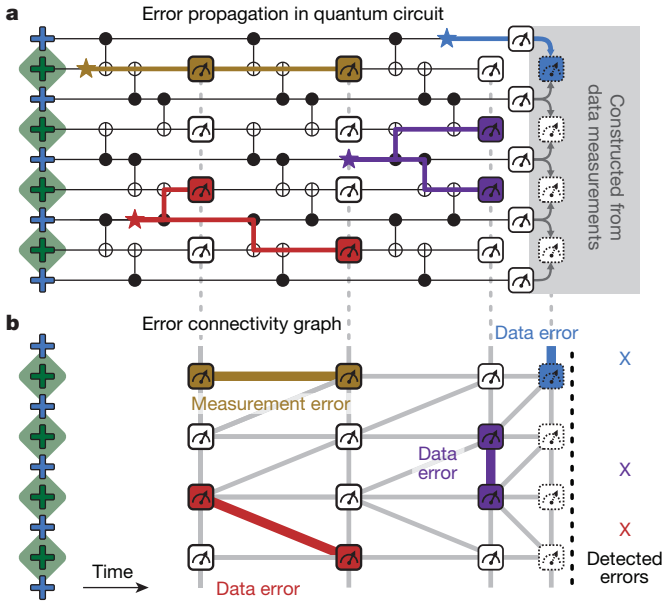

Figure 2 | Error propagation and identification. **a**, The quantum circuit for three cycles of the repetition code, and examples of errors. Errors propagate horizontally in time, and vertically through entangling gates. Different errors lead to different detection patterns: an error on a measurement qubit (gold) is detected in two subsequent rounds. Data qubit errors (purple, red, blue) are detected on neighbouring measurement qubits in the same or next cycle. Data errors after the last round (blue) are detected by constructing the final set of $\hat{Z}\hat{Z}$ eigenvalues from the data qubit measurements. **b**, The connectivity graph for the quantum circuit above, showing measurements and possible patterns of detection events (grey), see main text for details. The example detection events and their connections are highlighted, and the corresponding detected errors are shown on the right, which when applied, will recover the input data qubit state.

qubits are in the $|00\rangle$ or $|11\rangle$ state, the measurement qubit will report a string of identical values. If the data qubits are in the $|01\rangle$ or $|10\rangle$ state, the measurement qubit will report alternating values, as measurement is QND. Single data bit-flip errors make the measurement outcomes switch between these two patterns. For example, if the measurement outcomes for three cycles are 0, 0 and 1, this indicates a change from the identical to the alternating pattern in the last measurement, and hence a detection event. Explicitly, with m_t the measurement qubit outcome at cycle t and $\oplus$ the exclusive OR (XOR) operator, for each of the two patterns we have $b_t = m_{t-1} \oplus m_t = 0$ or 1. A detection event at cycle t is then identified when $D_t = b_{t-1} \oplus b_t = 1$.

We use minimum-weight perfect matching[23–25] to decode to physical errors, based on the pattern of detection events and an error model for the system. Intuitively, such matching connects detection events in pairs or to the boundary using the shortest total weighted path length. It is important to note that errors can lead to detection event pairs that span multiple cycles, necessitating the need for multi-round analysis as opposed to round-by-round (see Supplementary Information for details).

To study the ability of our device to preserve quantum states, we initialized the data qubits into a Greenberger–Horne–Zeilinger (GHZ) state, $\left[(|000\rangle + |111\rangle)/\sqrt{2}\right]$, and applied two rounds of the repetition code (Fig. 3). The algorithm is shown in Fig. 3a. Using quantum state tomography we measured the input density matrix ρ and find a GHZ state with fidelity $\mathrm{Tr}(\rho_{\mathrm{ideal}}\rho)$ of 82%, above the threshold of 50% for genuine entanglement[26]. After two repetition code cycles, we use tomography to construct the density matrices for each pattern of detection events. We find a state fidelity of 78% in the case of no detection events, indicating a retention of genuine quantum entanglement. In the case of two detection events, which indicate a likely data qubit error in the first cycle, we find elements away from the ideal positions. By applying the recovery operation in post-processing (a single bit-flip on the blue data qubit) we can restore the state. Energy relaxation, the most likely cause of the detected bit-flip error, induces both bit-flip and phase-flip errors. The bit-flip error is corrected and the diagonal terms are preserved, but any phase-flip error remains uncorrected, reducing the off-diagonal terms and fidelity to 59%. We note that genuine entanglement is preserved. Conditional tomography for every configuration can be found in Supplementary Information.

The data in Fig. 3 clearly show that the one-dimensional repetition code algorithm does not necessarily destroy the quantum nature of the state. It allows for preserving the quantum state in the case of no errors, and correcting bit-flip errors otherwise. This preservation is achieved purely through error detection and classical post-processing, like for the full surface code, avoiding the need for dynamic feedback with quantum gates. For the remainder, we investigate the logical basis states individually, as tomographic reconstruction cannot be done fault-tolerantly.

We now address the critical question of how well our implementation of the repetition code protects logical states over many cycles. The process flow is illustrated in Fig. 4a. We start by initializing the data qubits in either of the logical basis states: $|0_{\mathrm{L}}\rangle = |0..0\rangle$ or $|1_{\mathrm{L}}\rangle = |1..1\rangle$. We then run the repetition code algorithm for k cycles, and finish by measuring the state of all data qubits. We repeat this 90,000 times to gather statistics. The classical measurement results are converted into detection events, which are processed using minimum-weight perfect matching to generate corrections (see Supplementary Information). These corrections are then applied to the measured data qubit output

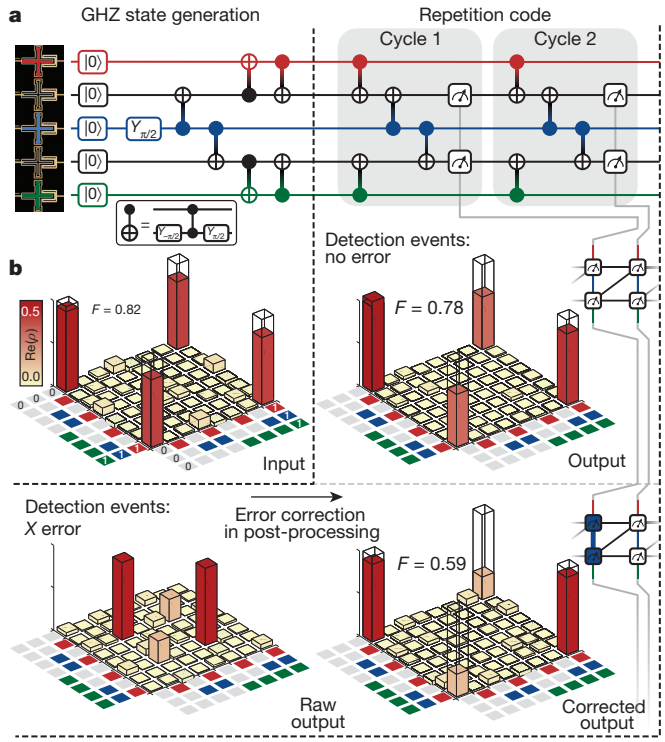

Figure 3 | Protecting the GHZ state from bit-flip errors. **a**, Quantum circuit for generating the GHZ state and two cycles of the repetition code. CNOT gates are physically implemented with controlled-phase (CZ) and single qubit gates. **b**, Quantum state tomography on the input (top left 'Input', left of black dashed line), and after the repetition code conditional on the detection events (between black dashed lines): we input a GHZ state with a fidelity (F) of 82%, and find, for the case of no detection events (top right 'Output', above grey dashed line), a 78% fidelity GHZ state. For the detection event connecting both measurement qubits (bottom left 'Raw output', below grey dashed line), indicating a likely bit-flip error on the central data qubit, we find that through correcting in post-processing by exchanging matrix elements we recover the major elements of the diagonal (bottom right 'Corrected output'). We also recover non-zero off-diagonal elements, indicating some bit-flip errors are coherent. Real parts are shown, $|\mathrm{Im}(\rho)| < 0.03$.

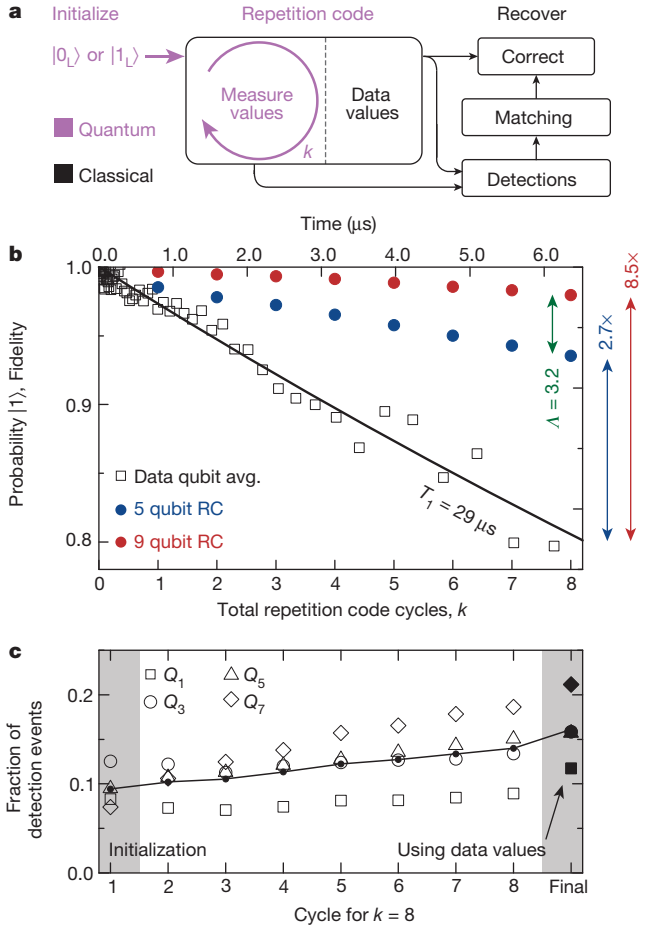

Figure 4 | Logical state preservation with the repetition code. **a**, Information flowchart of the repetition code. The data qubits are initialized into $|0_L\rangle$ or $|1_L\rangle$, and the repetition code is repeated k times. In post-processing, the measurement qubit outcomes are converted into detection events and matched to find likely errors, see Fig. 2. A successful recovery converts the measured data qubit state into the input state. **b**, Memory fidelity versus time and cycles for a single physical qubit (black) and the five- (blue) and nine- (red) qubit repetition code. Note that energy relaxation decays from a fidelity of 1 to 0, whereas the repetition code decays from a fidelity of 1 to 0.5. Five qubit data sampled from nine qubit data, see Supplementary Information. The average physical qubit lifetime ('data qubit avg.') is $T_1 = 29$ μs, and after eight cycles we see an improvement in error rate by a factor of 2.7 (blue arrow at right) for five qubits ('5 qubit RC'), and 8.5 (red arrow at right) for nine qubits ('9 qubit RC') when using the repetition code. This indicates a Λ parameter of 3.2 (green arrow) for our system after eight cycles. **c**, Average number of detection events per measurement qubit (open symbols), versus cycle number, for experiments consisting of eight cycles. We see an increasing average rate of detection events (black line) with increasing cycle number. This can be attributed to the statistically increasing number of odd parity $\hat{Z}\hat{Z}$ measurements, see text. Grey regions indicate initialization and final data qubit measurement.

to see if the input is recovered. Owing to the topological nature of errors in space and time, we either recover the logical state, or the bit-wise inverse (see Supplementary Information). The fidelity of the repetition code algorithm is defined by the success rate of this recovery. In our system, qubits naturally relax to $|0\rangle$, intrinsically making $|0_L\rangle$ more robust than $|1_L\rangle$. To balance these errors and to increase the worst-case lifetime of the system, we apply physical bit-flips to each data qubit at the end of each cycle. This logical flip is compensated for in software. In principle, bit-flip gates can be applied to a single physical qubit to reduce susceptibility to energy relaxation by at best a factor of two. However, this will introduce coherent gate errors. In order to quantify the reduction of logical errors with system size n, we have implemented the repetition code with five and nine qubits in total, corresponding to first- and second-order fault-tolerance.

In Fig. 4b we show the fidelity of the repetition code as a function of the number of cycles for five (blue) and nine (red) qubits. We also plot the probability of a $|1\rangle$ state idling for the same duration, averaged over the five data qubits (black). This allows for a direct comparison of single physical qubit error with the multi-qubit logical error. We find a reduced error of logical states after eight cycles as compared to a physical qubit; by a factor of 2.7 for five qubits and 8.5 for nine qubits. We also see a non-exponential fidelity decay for logical states, due to an increasing error rate with cycle number (Fig. 4c). This effect can be explained primarily by energy relaxation of measurement qubits, with a small contribution from state leakage. Initial logical states of all 0s or 1s have even parity for all $\hat{Z}\hat{Z}$ operators, maintaining the initial measurement qubit $|0\rangle$ state. A bit-flip error on a data qubit, statistically more likely with increasing cycle number, will cause the nearby $\hat{Z}\hat{Z}$ operators to have odd parity. This will flip measurement qubits between the $|0\rangle$ and $|1\rangle$ state at each cycle, making them susceptible to energy relaxation and hence increasing the rate of detection events (see Supplementary Information).

Figure 4 demonstrates state preservation through error correction. We emphasize that we correct errors that intrinsically arise from the environment. Additionally, we see larger repetition codes leading to greater error suppression. This is evidence for the system operating with fidelities above the repetition code threshold. As the error rates

grow with cycle number, the many-cycle behaviour of the repetition code must be explored to ensure that the system remains above threshold. The ratio of the errors for the $n = 1$ and $n = 2$ cases after eight cycles suggests $\Lambda = 3.2$, but larger system sizes are needed to infer this accurately for large n and verify that the logical error rate is suppressed exponentially as $\varepsilon_{\mathrm{logical}} \propto 1/\Lambda^{n+1}$, as desired.

Our demonstration that information can be stored with lower error in logical states than in single physical qubits shows that the basic physical processes required to implement surface code error correction are technologically feasible. We hope that our work will help to accelerate research into the many outstanding challenges that remain, such as the development of two-dimensional qubit arrays with scalable wiring and four-qubit QND parity checks, improving gate and measurement fidelities[27], and investigating the many-cycle behaviour of error correction schemes.

Received 22 November 2014; accepted 27 January 2015.

1. Shor, P. W. Scheme for reducing decoherence in quantum computer memory. *Phys. Rev. A* **52,** R2493–R2496 (1995).
2. Calderbank, A. R. & Shor, P. W. Good quantum error-correcting codes exist. *Phys. Rev. A* **54,** 1098–1105 (1996).
3. Steane, A. M. Error correcting codes in quantum theory. *Phys. Rev. Lett.* **77,** 793–797 (1996).
4. Bravyi, S. B. & Kitaev, A. Y. Quantum codes on a lattice with boundary. Preprint at http://arxiv.org/abs/quantph/9811052 (1998).
5. Raussendorf, R. & Harrington, J. Fault-tolerant quantum computation with high threshold in two dimensions. *Phys. Rev. Lett.* **98,** 190504 (2007).
6. Raussendorf, R., Harrington, J. & Goyal, K. Topological fault-tolerance in cluster state quantum computation. *New J. Phys.* **9,** 199 (2007).
7. Fowler, A. G., Mariantoni, M., Martinis, J. M. & Cleland, A. N. Surface codes: towards practical large-scale quantum computation. *Phys. Rev. A* **86,** 032324 (2012).
8. Cory, D. G. *et al.* Experimental quantum error correction. *Phys. Rev. Lett.* **81,** 2152–2155 (1998).
9. Knill, E., Laflamme, R., Martinez, R. & Negrevergne, C. Benchmarking quantum computers: the five qubit error correcting code. *Phys. Rev. Lett.* **86,** 5811–5814 (2001).
10. Chiaverini, J. *et al.* Realization of quantum error correction. *Nature* **432,** 602–605 (2004).
11. Reed, M. *et al.* Realization of three-qubit quantum error correction with superconducting circuits. *Nature* **482,** 382–385 (2012).
12. Chow, J. M. *et al.* Implementing a strand of a scalable fault-tolerant quantum computing fabric. *Nature Commun.* **5,** 4015 (2014).
13. Riste, D. *et al.* Detecting bit-flip errors in a logical qubit using stabilizer measurements. Preprint at http://arxiv.org/abs/1411.5542 (2014).
14. Nigg, D. *et al.* Quantum computations on a topologically encoded qubit. *Science* **345,** 302–305 (2014).
15. Córcoles, A. *et al.* Detecting arbitrary quantum errors via stabilizer measurements on a sublattice of the surface code. Preprint at http://arxiv.org/abs/1410.6419 (2014).
16. Schindler, P. *et al.* Experimental repetitive quantum error correction. *Science* **332,** 1059–1061 (2011).
17. Sun, L. *et al.* Tracking photon jumps with repeated quantum non-demolition parity measurements. *Nature* **511,** 444–448 (2014).
18. Bombin, H. & Martin-Delgado, M. Quantum measurements and gates by code deformation. *J. Phys. A* **42,** 095302 (2009).
19. Barends, R. *et al.* Superconducting quantum circuits at the surface code threshold for fault tolerance. *Nature* **508,** 500–503 (2014).
20. Jeffrey, E. *et al.* Fast accurate state measurement with superconducting qubits. *Phys. Rev. Lett.* **112,** 190504 (2014).
21. Barends, R. *et al.* Coherent Josephson qubit suitable for scalable quantum integrated circuits. *Phys. Rev. Lett.* **111,** 080502 (2013).
22. Fowler, A. G., Sank, D., Kelly, J., Barends, R. & Martinis, J. M. Scalable extraction of error models from the output of error detection circuits. Preprint at http://arxiv.org/abs/1405.1454 (2014).
23. Edmonds, J. Paths, trees, and flowers. *Can. J. Math.* **17,** 449–467 (1965).
24. Edmonds, J. Maximum matching and a polyhedron with 0,1-vertices. *J. Res. Natl Bur. Stand. B* **69,** 125–130 (1965).
25. Fowler, A. G. Minimum weight perfect matching of fault-tolerant topological quantum error correction in average O(1) parallel time. *Quant. Inform. Comput.* **15,** 0145–0158 (2015).
26. Gühne, O. & Seevinck, M. Separability criteria for genuine multiparticle entanglement. *New J. Phys.* **12,** 053002 (2010).
27. Harty, T. *et al.* High-fidelity preparation, gates, memory and readout of a trapped-ion quantum bit. *Phys. Rev. Lett.* **113,** 220501 (2014).

Supplementary Information is available in the online version of the paper.

Acknowledgements We thank A. N. Korotkov and D. L. Moehring for discussions, and P. Duda for help with photomasks and photolithography. This work was supported by the Office of the Director of National Intelligence (ODNI), Intelligence Advanced Research Projects Activity (IARPA), through Army Research Office grants W911NF-09-1-0375 and W911NF-10-1-0334. All statements of fact, opinion or conclusions contained herein are those of the authors and should not be construed as representing the official views or policies of IARPA, the ODNI or the US Government. Devices were made at the UC Santa Barbara Nanofabrication Facility, a part of the US NSF-funded National Nanotechnology Infrastructure Network, and at the NanoStructures Cleanroom Facility.

Author Contributions J.K. and R.B. designed the sample and performed the experiment. A.G.F. and J.M.M. designed the experiment. J.K., R.B. and A.M. fabricated the sample. A.G.F., J.K. and R.B. analysed the data. J.K., R.B., A.G.F. and J.M.M. co-wrote the manuscript. All authors contributed to the fabrication process, experimental set-up and manuscript preparation.

Author Information Reprints and permissions information is available at www.nature.com/reprints. The authors declare no competing financial interests. Readers are welcome to comment on the online version of the paper. Correspondence and requests for materials should be addressed to J.K. (julian@physics.ucsb.edu) or J.M.M. (martinis@physics.ucsb.edu).